

# Ultra-High-Intensity Laser Propagation Through Underdense Plasma

Z. Najmudin, M. Tatarakis, K. Krushelnick, E. L. Clark, V. Malka, J. Faure, and A. E. Dangor

**Abstract**—Picosecond resolution shadowgraphy is a powerful tool for measurement of high-intensity laser propagation instabilities through underdense plasma. It is shown that as the plasma density increases, the laser beam is subject to severe filamentation instabilities—likely due to the effect of stimulated Raman side-scattering. At higher plasma densities, scattering and absorption are so severe that the propagation distance of the high intensity laser pulse is reduced.

**Index Terms**—Intense laser plasma.

RECENT experiments have demonstrated the potential of using high-intensity laser-produced plasmas as a source of high-energy (multiMeV) electrons [1]–[3]. These electrons are accelerated by electric fields associated with large amplitude electron plasma waves generated in the plasma by the intense laser pulse. In previous experiments,  $10^{12}$  electrons accelerated to energies above 2 MeV, with a maximum energy of up to 120 MeV [4] having been measured.

In this paper, we report results from recent experiments in which propagation and scattering instabilities of high-intensity laser pulses in underdense plasmas were examined. In particular, we have used picosecond shadowgraphy to measure the complex filamentation and side-scattering instabilities which occur at extreme laser intensities.

These experiments were carried out at the VULCAN Facility, RAL, Chilton, U.K. VULCAN produces pulses of power up to 50 TW in a duration of 0.9–1.2 ps at a wavelength of  $1.054 \mu\text{m}$ . The laser pulse was focused into a gas jet using an  $f/4$  off axis parabolic mirror. In vacuum, the laser could be focused to a peak intensity of greater than  $10^{19} \text{ W/cm}^2$ . Helium was used as the target gas and the plasma had an electron density up to about  $5 \times 10^{19} \text{ cm}^{-3}$ .

The plasma is formed by optical field ionization of the gas by the front of the intense laser beam. In addition, spatially resolved measurements of the Raman side-scatter were taken. For shadowgraphy, a second unfocused frequency-doubled probe beam was passed transversely through the interaction. The probe was derived from the same source as the main beam to ensure jitter-free timing. Gradients of density within the plasma deflect the probe light so that regions of plasma can be clearly imaged

with high temporal and spatial resolution. The duration of the probe beam was about 3 ps and was synchronized to the passage of the main pulse through the plasma.

A set of shadowgrams is shown for a variety of densities in Fig. 1. The lowest density at which signature of the propagation can be observed is around  $3 \times 10^{18} \text{ cm}^{-3}$  [Fig. 1(A)]. On all of these shots the laser has been focused at the edge of the gas jet to ensure that the interaction occurs at the highest intensities possible. This shadowgram shows the “fan” shaped plasma created by a defocusing laser beam of cone angle  $\approx f/4$ .

Doubling the plasma density [Fig. 1(B)] does not change the shadowgram greatly, however, there is a marked increase in the amount of Raman side-scatter. Striations can also be clearly seen in the shadowgram of Fig. 1(B) within the cone of the plasma. The laser intensity is highly nonuniform in the outward going cone, leading to slight variations in plasma density. A darker striation can be noticed near the start of the propagation. This is caused by the “blow-out” or cavitating channel generated by ponderomotive/relativistic self-focusing of the laser beam.

The self-focusing channel is even clearer in Fig. 1(C). Indeed, initially all of the laser light seems to be traveling in the forward direction, and the cone shape seen in Figs. 1(A) and (B) is absent. However, at this higher density, the initial channel is shorter and appears to end abruptly, after which the laser beam defocuses in the usual fan. Initially the side scattering is weak, but becomes extremely intense and spatially localized to the end of the channel. Indeed, the fact that the channel end is correlated to this intense scattering is further corroborated by the appearance in the shadowgram of ionizing filaments at large angles. These filaments originate at the end of the deep channel, and propagate away almost orthogonally to the driver beam.

This behavior is more pronounced in the final image [Fig. 1(D)]. At this density, the central channel created in the shadowgram is clearer, but again ends in an intense burst of side scatter. Afterwards, the whole beam defocuses naturally, but with a greater divergence than at low densities. All of the propagation lengths are shorter at this density both from the shadowgram, and from Raman side-scatter. This indicates that the beam is heavily absorbed. Similar conditions have been shown to be the most efficient for conversion of laser energy to fast electrons [4].

In conclusion, the effect of Raman side-scatter correlated with observation through plasma probing of channel formation due to relativistic self-focusing, has been observed. At the highest densities, it is only with the termination of strong channeling that one sees the onset of intense Raman side-scatter.

Manuscript received July 17, 2001; revised November 19, 2001. This work was supported by the E.P.S.R.C., U.K.

Z. Najmudin, M. Tatarakis, K. Krushelnick, E. L. Clark, and A. E. Dangor are with Department of Physics, Blackett Laboratory, Imperial College, London SW7 2BZ, U.K. (e-mail: kmkr@ic.ac.uk).

V. Malka and J. Faure are with Laboratoire pour l’Utilisation des Lasers Intenses, Ecole Polytechnique, Palaiseau, France.

Publisher Item Identifier S 0093-3813(02)03326-X.

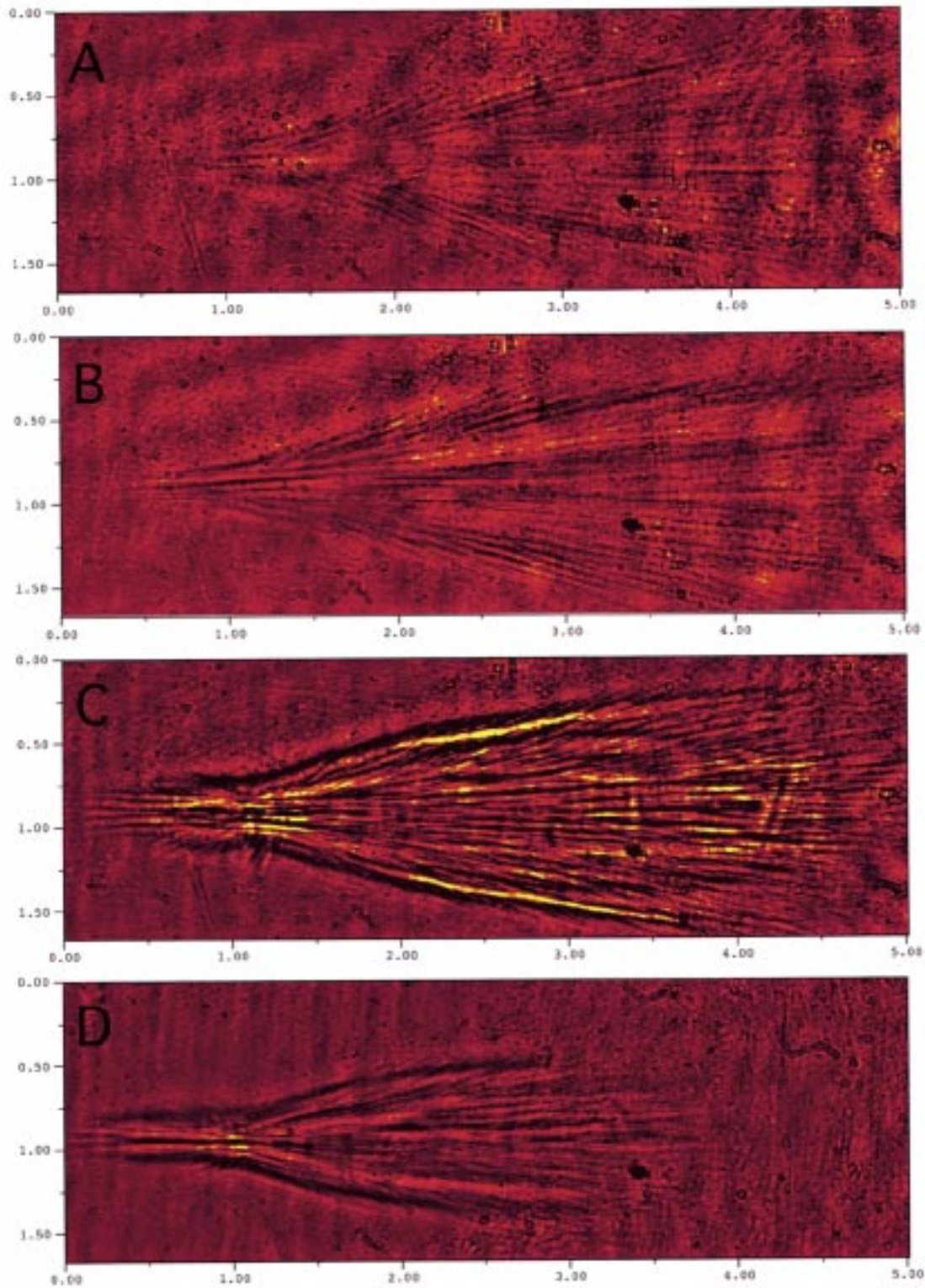


Fig. 1. Picosecond shadowgrams of intense laser propagation through underdense plasma. The laser has a peak intensity of  $\sim 10^{19}$  W/cm<sup>2</sup> and is incident from the left. The photograph width corresponds to 6 mm. (A)  $n_e = 3.5 \times 10^{18}$  cm<sup>-3</sup>; (B)  $n_e = 7.0 \times 10^{18}$  cm<sup>-3</sup>; (C)  $n_e = 2.9 \times 10^{19}$  cm<sup>-3</sup>; (D)  $n_e = 3.5 \times 10^{19}$  cm<sup>-3</sup>.

#### REFERENCES

- [1] T. Tajima and J. M. Dawson, "Laser electron accelerator," *Phys. Rev. Lett.*, vol. 43, p. 267, 1979.
- [2] P. Sprangle, E. Esarey, A. Ting, and G. Joyce, "Laser wakefield acceleration and relativistic optical guiding," *Appl. Phys. Lett.*, vol. 53, p. 2146, 1988.
- [3] E. Esarey, P. Sprangle, J. Krall, and A. Ting, "Overview of plasma-based accelerator concepts," *IEEE Trans. Plasma Sci.*, vol. 24, pp. 252–288, Apr. 1996.
- [4] M. I. K. Santala, Z. Najmudin, E. L. Clark, M. Tatarakis, K. Krushelnick, A. E. Dangor, V. Malka, J. Faure, R. Allott, and R. J. Clarke, "Observation of a hot high-current electron beam from a self-modulated laser wakefield accelerator," *Phys. Rev. Lett.*, vol. 86, pp. 1227–1230, 2001.